C.L. Bottasso, P. Bortolotti, A. Croce, F. Gualdoni
Integrated Aero-Structural Optimization of Wind Turbines
Multibody System Dynamics, Vol. 38, N. 4, 2016, p. 317-344
doi:10.1007/s11044-015-9488-1

Multibody System Dynamics manuscript No.
(will be inserted by the editor)

Integrated aero-structural optimization of wind turbine rotors

C.L. Bottasso · P. Bortolotti · A. Croce · F. Gualdoni

November 2015

Abstract The present work describes methods for the integrated aero-structural optimization of wind turbine rotors. Goal of the algorithms is to identify the structural and aerodynamic rotor design characteristics that achieve the minimum cost of energy for a given wind turbine configuration. Given the strong couplings that exist between aerodynamic and structural design choices, the methods are formulated so as to address both problems simultaneously in an integrated manner, resulting in tools that may help avoid suboptimal solutions or lengthy design loops.

All methods considered herein use the same high fidelity multibody aeroservoelastic simulation environment and operate the design according to standard certification guidelines. The methods however differ in the way the optimization is conducted, realizing different tradeoffs amongst computational efficiency, generality, level of automation and overall robustness.

The proposed formulations are exercised on the design of a conceptual 10 MW horizontal axis wind turbine, illustrating the main characteristics of the various methods.

Keywords Wind turbine · Blade design · Multibody dynamics · Aero-structural optimization · Aeroservoelasticity · Multidisciplinary optimization

1 Introduction

The design of wind turbine rotors is an inherently multidisciplinary activity that requires the complex integration of different optimization processes.

In fact, on the one hand the external shape of a wind turbine blade is driven by aerodynamic considerations that ultimately aim at maximizing the power extraction from wind. In

C.L. Bottasso
Wind Energy Institute, Technische Universität München, D-85748 Garching b. München, Germany, and
Dipartimento di Scienze e Tecnologie Aerospaziali, Politecnico di Milano, I-20156 Milano, Italy.
E-mail: carlo.bottasso@tum.de

P. Bortolotti
Wind Energy Institute, Technische Universität München, D-85748 Garching b. München, Germany.

A. Croce · F. Gualdoni
Dipartimento di Scienze e Tecnologie Aerospaziali, Politecnico di Milano, I-20156 Milano, Italy.

principle, this would require the use of thin aerodynamic profiles of high efficiency and the design of a low solidity rotor. On the other hand, structural efficiency considerations lead to the use of high thickness airfoils, especially close to the blade root. This, in conjunction with an increased chord and hence solidity, makes it easier to achieve enough blade stiffness to meet clearance and/or frequency placement constraints, while limiting weight and reducing the need for high performance materials.

The Cost of Energy (CoE) is the figure of merit that should be minimized in order to guarantee a competitive generation of electricity from wind. CoE depends, among other factors, both on the aerodynamic efficiency (which affects the Annual Energy Production, or AEP) and on the cost of the rotor (which depends on weight and materials, for a given manufacturing technology). Therefore, when designing rotors that try to achieve the best possible CoE, it is important to account for all subtle couplings that exist among the aerodynamic and structural aspects of the problem. While this is very well known to industry, at the moment the ability to simultaneously size a rotor both from the aerodynamic and structural points of view in an automatic fashion is still lacking. Current best design procedures are based on successive iterations between the aerodynamic and structural designs, guided by practice and experience. Although the knowledge and experience of a good engineer cannot be replaced by algorithms, methods that can assist in the process by accounting for all intricate couplings that exist among the various involved subdisciplines may be of great help in exploring the solution space and in eventually arriving to sound design solutions.

The recent scientific literature shows a marked interest towards the development of tools for the optimization of wind turbines, and of wind turbine rotors in particular. For example, Ref. [1] analyzed the effect of using different cost functions for a same design optimization problem, concluding that CoE is the most appropriate figure of merit. This study also highlighted the importance of high fidelity cost models, which are however generally unavailable in the public domain. The integration of the aerodynamic and structural designs were recently considered in studies conducted by some of the presents authors [2]. Using aeroservoelastic models, procedures were developed to determine the chord and twist distribution of the blade and the sizing of all its main structural components, while satisfying constraints on ultimate and fatigue admissibles, stiffness (frequency placement and/or tower clearance), and geometry. Recently, Ref. [3], using somewhat lower fidelity models, added the capability of simultaneously designing also the airfoil shapes, this way performing a genuine free-form three-dimensional optimization of the rotor blade.

Several other studies are reported in the literature, and differ for the fidelity of the tools used and their level of integration and automation. In Ref. [4], a multi-level framework is developed to coordinate multiple optimizations, involving different disciplines and modeling techniques. The ultimate goal is to perform a top-level optimization that provides a feasible aero-structural design according to all disciplines. A simultaneous design of aerodynamic properties and bend-twist coupling characteristics of the blade is carried out in Ref. [5]. Airfoil shapes, chord and twist distribution and degree of structural coupling are considered as optimization variables, resulting in a reduction in CoE through a decrease in loads at constant aerodynamic performance. A site-specific aero-structural design is considered in Ref. [6], where the effects of the different wind characteristics available at different sites lead to different optimal design solutions. Reference [7] considers an optimal coupling between rotor aerodynamic performance and rotor and tower structures, this way achieving a reduction in CoE, while at the same time trying to balance between model accuracy and computational cost. If CoE is not used as the figure of merit, multi-objective optimization techniques can be applied. An example is reported in Ref. [8], where aerodynamic and struc-

tural properties are optimized by considering as objective functions turbine thrust, AEP and blade mass.

Aim of this work is to propose optimization algorithms that perform an *integrated aero-structural* design of a wind turbine rotor by minimizing a CoE model. All methods considered here make use of high fidelity simulation models, that include a 2D cross sectional analysis model, a multibody aeroservoelastic model, and detailed 3D FEM models. The design is based on current industrial standard procedures, which include the certification guidelines and Design Load Cases (DLCs) prescribed by the International Electrotechnical Commission (IEC) [9] and by Germanischer Lloyd (GL) [10]. All desired features of the solution are enforced by means of appropriate constraints appended to the optimization problem. Aerodynamic constraints include maximum blade tip speed, on account of noise or compressibility, maximum chord for transportability, in addition to a variety of geometric constraints to ensure smoothness or specific requirements on the blade shape, as for example conditions on spanwise tapering or solidity. Structural constraints include stress, strain and fatigue allowables, but also the placement of blade natural frequencies to avoid resonant conditions, tower clearance to avoid blade strikes, as well as a variety of geometric constraints to enforce manufacturing, technological and other conditions. Within this simulation-based constrained optimization environment, in this work three different aero-structural approaches are considered, realizing three different compromises on computational efficiency, generality, level of automation and robustness. The three algorithms are then applied to the design of a conceptual 10 MW wind turbine, illustrating the main features, similarities and differences of the proposed methods.

The paper is organized as follows. Section 2 presents the wind turbine simulation environment in §2.1, as well as the purely aerodynamic (§2.2) and structural (§2.3) optimizations that represent the pillars of the integrated algorithms. This part of the work is closed by §2.4, where a simple example is used to illustrate the shortcomings of uncoupled aerodynamic and structural optimizations. The three proposed aero-structural optimization algorithms are discussed in Sect. 3: §3.1 presents the simplest approach, based on pre-assumed aerodynamic shapes; §3.2 discusses a method based on two nested aerodynamic/structural optimization loops; finally, §3.3 presents a monolithic approach where a load updating strategy is used to contain the computational cost. Results obtained by the application of the different aero-structural approaches are illustrated in Sect. 4. At first, §4.1 presents a baseline configuration of a large rotor, used to provide reference parameters and performance as well as an initial configuration to be used as starting guess for all new methods. Next, §4.2 illustrates and analyzes the results obtained by the three proposed algorithms. Concluding remarks, recommendations and an outlook for future work are finally given in Sect. 5.

2 Simulation models and monodisciplinary optimizations

The wind turbine design optimization environment described in this work is implemented in the software tool `Cp-Max` (Code for Performance Maximization). The present section describes the simulation models used by `Cp-Max`, as well as the monodisciplinary purely-aerodynamic and purely-structural optimization procedures that it implements. This will form the basis for the explanation of the multidisciplinary optimization algorithms described in the next section.

2.1 Wind turbine aeroservoelastic modeling

Optimization techniques of complex aeroservoelastic system, such as wind turbines, are based on simulation models, which must able to represent the behaviour of the machine to a sufficient degree of fidelity in all relevant operating conditions encountered throughout its lifetime [9, 10]. The post-processing of such analyses in turn enables the evaluation of all necessary quantities that appear in the figure of merit and constraints of a design problem.

In the present work, simulation models are implemented with the code `Cp-Lambda` (Code for Performance, Loads, Aeroelasticity by Multi-Body Dynamic Analysis [13]). Originally developed for rotorcraft applications, the software has been validated with respect to other industrial simulation programs, wind tunnel experimental results and field measurements.

`Cp-Lambda` is an aeroservoelastic simulator based on a multibody formulation for flexible systems with general topologies. The code features a library of elements, which include rigid bodies, nonlinear flexible elements, joints, actuators and aerodynamic models. Sensor and control elements enable the implementation of generic control laws. The index-3 formulation is expressed in terms of Cartesian coordinates, while constraints are enforced by scaled Lagrange multipliers [14].

Rotor blades and tower are described by nonlinear geometrically exact shear and torsion deformable beam models, based on an optionally fully populated stiffness on account of couplings due to the use of anisotropic composite materials [15]. Flexible components are discretized in space by the finite element method, leading to a system of differential algebraic equations in the time domain. Time integration is performed by a non-linearly unconditionally stable scheme that includes high frequency dissipation by energy decay [16].

The blade aerodynamic characteristics are defined by lifting lines, which include the spanwise chord and twist distributions as well as sectional aerodynamic coefficients, given in tabular form and parameterized in terms of the Reynolds number. The effects of the wake are modelled by a classical blade-element momentum (BEM) model based on annular stream tube theory with wake swirl and unsteady correction [17], or by the dynamic inflow model of Refs. [18, 19]. The aerodynamic description is completed by root and blade tip losses, unsteady aerodynamic corrections, dynamic stall, 3D blade root delayed stall and rotor-tower interference models. The wind field includes deterministic gusts and turbulent time histories, which may be obtained by the open-source software `TurbSim` [20].

The machine is governed over its entire operating range by controllers interfaced with the wind turbine model by external dynamic libraries. A supervisory unit manages the machine behavior by switching among different operating states and handling emergencies. Pitch and torque are handled by suitable controllers operating in closed-loop with the machine on the basis of data supplied by sensor models.

All operative conditions prescribed by international standards can be analyzed within the software environment [9, 10]. In addition to transient simulations, available analysis types also include static analyses, used for determining static solutions or approximate steady state configurations to be used as initial conditions, as well as eigenanalyses about linearized trim points.

2.2 Aerodynamic optimization of rotor blades

The purely aerodynamic optimization of the wind turbine rotor consists here in identifying the optimal chord and twist distributions to achieve the maximum AEP, for a given set of airfoils. A more general technique that does not assume a preselected set of airfoils is

described in Ref. [3]. A set of non-linear constraints is included in the optimization problem to specify additional required features of the solution.

The aerodynamic optimization problem can be expressed as follows:

$$\textbf{Function } (\boldsymbol{p}_a^*, P_y^*) = \texttt{MaxAEP}(\boldsymbol{p}_a, \boldsymbol{p}_s, D): \tag{1a}$$

$$P_y^* = \max_{\boldsymbol{p}_a} \texttt{AEP}(\boldsymbol{p}_a, \boldsymbol{p}_s, D) \quad \left(\text{and } \boldsymbol{p}_a^* = \arg\max_{\boldsymbol{p}_a}(AEP)\right), \tag{1b}$$

$$\text{s.t.:} \quad \boldsymbol{g}_a(\boldsymbol{p}_a) \leq \boldsymbol{0}, \tag{1c}$$

$$v_{\text{tip}} \leq v_{\text{tip}_{\text{max}}}. \tag{1d}$$

Here and in the following, functions are indicated with the notation

$$(O) = \texttt{FunctionName}(I), \tag{2}$$

where I are the input variables, while O the output ones.

In Eq. (1), $\boldsymbol{p}_a$ and $\boldsymbol{p}_s$ are vector arrays containing, respectively, the aerodynamic and structural variables of the optimization problem. $\boldsymbol{p}_a$ is the stacking of $\boldsymbol{p}_{a,t}$ and $\boldsymbol{p}_{a,c}$, which are the two vectors describing the shape functions that modify twist and chord distributions, respectively. The variables $\boldsymbol{p}_s$ define the structural configuration as shown in §2.3. Even if they are kept constant by `MaxAEP` algorithm, they are explicitly reported to point out that an optimal aerodynamic configuration is affected by the structural flexibility.

In the same equation, D is a list of given data:

$$D = \{P_r, V_{\text{in}}, V_{\text{out}}, R, H, AF, C, v_{\text{tip}_{\text{max}}}, \ldots\}. \tag{3}$$

The list includes, among other quantities, the rated power P_r, the cut-in and cut-out wind speeds V_{in} and V_{out}, the rotor radius R, the tower height H, the list AF of AirFoils used along the blade span, the wind turbine class C and the maximum tip speed $v_{\text{tip}_{\text{max}}}$. The maximum AEP, denoted P_y^*, is obtained at the corresponding value of the aerodynamic design parameters $\boldsymbol{p}_a^*$. Finally, $\boldsymbol{g}_a$ represents a set of linear and non-linear constraints of variables $\boldsymbol{p}_a$. The list of constraints is flexible and can be tailored to specific needs, but it generally includes values for maximum chord, upper bounds for the first and/or second derivatives of chord and twist distributions, a tapering parameter and minimum/maximum rotor solidity values.

The optimization routine `MaxAEP` is implemented in MATLAB [21]. The core of the code is the gradient based optimization function `fmincon`, which uses a Sequential Quadratic Programming (SQP) algorithm, allowing for an efficient handling of constraint equations [22]. Gradients are computed automatically by finite differences. Since the optimization variables are related to dissimilar data, i.e. chord and twist angle, they are made nondimensional before gradient evaluation. The nondimensional scaling constants are related to the user-defined upper bounds and the imposed perturbation of finite difference is 2% of the resulting nondimensional value.

A gradient based approach is used here because the problem is expected to be smooth. In fact the spanwise aerodynamic shape and property distributions of the blade are smooth by construction. In addition, in the neighborhood of the optimal condition, assuming as customary a steady axial flow, the blade operates away from stall, and hence the aerodynamic loads exhibit a regular behavior with respect to the angle of attack. Therefore, because of the smoothness of the input data and of the loads that characterize the optimal configuration around the optimal operating condition, one may perform the design using gradient based techniques. Clearly, for this to work effectively, the initial guess has to be within the basin of attraction of the algorithm.

The evaluation of the cost function of routine `MaxAEP` consists of several steps. Firstly, the lifting lines describing the aerodynamic properties of the blade model in `Cp-Lambda` are updated based on the current design values $\boldsymbol{p}_a$. To limit the number of degrees of freedom, multiplicative shape functions based on splines are used to deform a given baseline configuration. Static simulations are then run in steady wind conditions to evaluate the aerodynamic performance of the machine for a two-dimensional grid of parameters, which are chosen as the tip speed ratio λ and the blade pitch angle β. These simulations take into account the aeroelastic effects of the flexible bodies of the entire wind turbine model and include the computation of aerodynamic, inertial and gravitational loads. Optionally, one may repeat the analyses for varying values of the wind speed, on account of the different deformations experienced by the machine throughout its operational range. These simulations represent snapshots of the wind turbine, with its rotor at a certain given azimuthal position, under the aerodynamic and inertial loads that correspond to a steady rotation at a prescribed rotor speed. While this is an approximation of the actual time-periodic response of the machine in steady wind conditions, when repeated and averaged over a few different rotor azimuthal positions, it provides for a rapid and accurate evaluation of the mean value solution by means of simple static simulations.

The aerodynamic performance is then evaluated by extracting internal forces at the hub, which yield thrust force and torsional moment. By nondimensionalizing these values, one obtains the power C_P and thrust C_T coefficients, as functions of λ, β and optionally of the wind speed V, which are then stored in look-up tables. Based on the C_P table, the regulation trajectory is computed, defining the control parameters for regions II and III, which are the operating regions between V_{in} and rated wind speed V_{r} and between V_{r} and V_{out} respectively. The transition region II$^1/_2$ [23] may also be required in presence of an active tip speed constraint and it is a function of the rated speed, which in turn depends on the solidity of the rotor. Therefore, during the iterations of the aerodynamic optimization loop, the extent of the three regions, and particularly the one of region II$^1/_2$, may change based on the variations of the aerodynamic design parameters $\boldsymbol{p}_a$.

The whole process to compute the regulation trajectory is performed twice: a first run on a coarse λ-β grid allows one to identify the λ of maximum C_P and the region around which the machine typically operates within its wind speed range; next, a second run is performed on a more refined grid around the values of interest. This allows for a more accurate computation of the performance curves while limiting the computational cost.

Once the regulation trajectory has been computed, the power curve is then readily obtained. By weighting it with the Weibull distribution for the prescribed wind turbine class [9, 10], one finally obtains the AEP.

Function `MaxAEP` has shown good robustness in several practical applications, and convergence is generally achieved in just a few iterations. The computational cost of the aerodynamic optimization routine is limited compared to the other optimizations described later on in this work.

2.3 Structural optimization of rotor blades and tower

This paragraph describes the formulation and solution of the monodisciplinary structural optimization problem for an assigned aerodynamic shape. Due to the complexity of the problem, the description is organized in two separate parts: §2.3.1 gives a first general overview of the structural optimization problem, followed by §2.3.2, which gives a more detailed and formal description.

2.3.1 *Overview of monodisciplinary structural optimization*

The structural optimization procedure aims at obtaining the lightest structure that satisfies a set of design requirements, for a given aerodynamic configuration. The procedure can size the sole rotor for a given tower, the sole tower for a given rotor, or it can consider the more general problem of simultaneously sizing rotor and tower [12]. A simultaneous sizing can be of interest in certain situations, as each one of the two components affects the other, mainly through the blade-tower clearance constraint to avoid strikes, as well as through the placement of the respective natural frequencies.

The algorithm operates at multiple levels. A "coarse" aeroservoelastic level is based on quasi-3D models of the entire machine, comprising of a flexible beam multibody model supplemented with 2D sectional models. The load analysis is performed at this level, yielding both fatigue and ultimate loads at all points of interest on the structure. 3D finite element models are then used to refine the coarse solution. The overall organization of the algorithm is reported in Fig. 1.

A parameterized model of the blade structure, and optionally of the tower, is defined by choosing optimization variables at a chosen number of control stations. The model characteristics in between control stations are obtained by interpolation using shape functions.

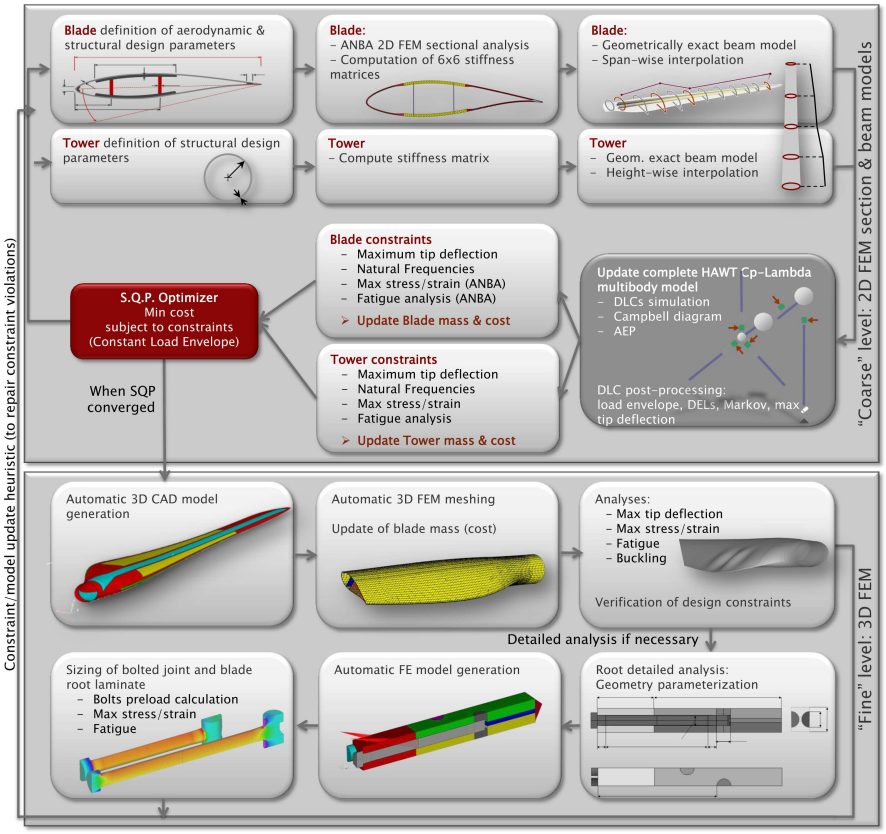

Figure 1 Multi-level structural blade-tower optimization for given aerodynamic shape

The optimization variables are linearly interpolated while the geometric data, such as blade chord and twist angle, are interpolated by cubic splines. The blade optimization variables can be chosen among the thickness of the external shell, spar caps, shear webs, as well as leading and trailing edge reinforcements. A classical tubular solution is considered for the tower and its structural design parameters are diameter and wall thickness at selected stations. Blade properties are computed by a finite element cross sectional analysis conducted with the software `ANBA`, implementing the theory of Ref. [24]. The discretization is performed by orthotropic isoparametric panels and the formulation leads to fully populated stiffness matrices, accounting for all possible couplings that may arise due to the use of anisotropic composite materials. Moreover, recovery relationships are computed that allow for the evaluation of the stress and strain distributions on the blade sections. Due to the simpler geometry of the tower, the stiffness properties and the stress/strain distributions are obtained by classical analytical theory for conical hollow beams. All structural properties computed in this way are then used to define the corresponding beams in the `Cp-Lambda` model. The definition of the multi-body model implies the evaluation of the structural properties at different location of the blade span, related to the characteristics of the beams mesh. This evaluation is performed by a linear interpolation of the sectional data provided by the user.

In turn, the multibody model is used for running all necessary DLCs, which typically include those specified by international standards [9, 10]. The quantities necessary for sizing are obtained automatically by post-processing routines. Ultimate stress and strain distributions are evaluated from the load envelope by `ANBA` on each verification section. A rainflow counting algorithm and damage accumulation rules are used to estimate the fatigue life from stress time histories. Resonant conditions can be avoided by constraining the placement of chosen modes in specific frequency ranges. The clearance between blade tip and tower is also evaluated, by searching the most demanding condition within all DLCs. All these quantities, together with other desired geometrical conditions used for prescribing manufacturing and technological requirements, are expressed as inequality constraints, which are enforced during the optimization procedure.

As the procedure performs a detailed design of all main structural components of blades and tower, a detailed bill of materials is readily obtained. This enables the evaluation of the cost of such components, at least for given manufacturing technologies, which in turn enters into the definition of the Initial Capital Cost (ICC) [25]. The cost of other components, such as for example bearings or parts of the pitch system, might be affected by changes in the design, and this can be taken into account if appropriate cost models of such subcomponents are available. Because in the monodisciplinary optimization the aerodynamic shape is held fixed, AEP does not change in an appreciable manner for different structural sizing solutions. Therefore the ICC (as opposed to the CoE that will be used later on for the more general aero-structural optimization) can be assumed as the figure of merit for the structural sizing problem.

Blade mass is computed by considering also different types of nonstructural mass contributors, such as adhesive, resin uptake, bonding plies and the presence of a lightning protection system. The core thickness distribution is estimated by analytical formulas, as reported in Ref. [26], and it is included in the nonstructural mass evaluation. Tower mass is computed by considering the flanges connecting neighboring sections and nonstructural masses distributed along the tower height on account of additional components, such as ladders, cables and an elevator, if present.

A SQP algorithm is used to solve numerically the structural sizing problem. During the optimization, loads are temporarily kept constant (frozen), to reduce the computational

effort and increase the regularity of the problem [2,12]. In fact, while smoothness of the merit function and constraints is a requirement when gradient based optimization algorithms are used, a non-smooth behavior can be induced by the ultimate loads. The selection of the most severe conditions is carried out for each load component by searching maxima and minima within all load time histories of the considered set of DLCs. During design, such extreme values might change abruptly, for example when jumping from one dominating DLC to another.

By freezing the load envelope, one temporarily renders the problem smooth, and hence solvable by a gradient based technique. However, one is also clearly forced to update the loads, in order to reflect changes due to the changed design of the blade. This is done by an external iteration: when an optimal solution is found by the SQP algorithm at frozen loads, the aeroelastic wind turbine model is updated and loads are re-evaluated. The process of load freezing and optimization is repeated until convergence, which is usually obtained in just a couple of iterations. Experience has shown that this procedure works better than non-gradient-based methods, because of the large number of constraints that are typically needed for formulating the design problem.

The coarse aeroelastic solution is improved at a "fine" level, as shown in Fig. 1. A 3D CAD blade model is generated automatically considering all the constitutive elements of the blade, i.e. spar caps, external skin, shear webs and reinforcements. The CAD model is then meshed by orthotropic shell elements, and all constraints enforced at the coarse level are verified on the resulting finite element mesh. The 3D FEM results are used to correct the constraints applied during the coarse aeroelastic optimization. This is a heuristic, but simple and effective, way to include at the coarse level the solution features that only a complete 3D model can capture. Corrections are usually obtained at the beginning and end of the shear webs and around the maximum chord span, i.e. in those parts of the blade where beam theories are not accurate enough. This step in the analysis allows for a more precise sizing of structural details that, despite their limited extension, directly affect the blade configuration. The 3D FEM model is also used for the verification of the buckling constraints, which may lead to corrections of the required core thickness and hence to an update of the total blade mass. A detailed description of the constraint scaling process and of the update of the figure of merit is given in Ref. [12].

Finally, one may also create a 3D FEM model of the blade root bolted joint to define the laminate thickness in the root region, which, due to its considerable thickness, may typically have a significant effect on the blade total mass. A classical T-Bolt configuration is shown in Fig. 1, but the approach implemented here can handle different typologies, as for example a threaded insert solution. A solid CAD geometry is generated and meshed, accounting for symmetry to reduce the size of the problem, using `Altair Hypermesh` [27] with scripts in `Tcl` [28]. The resulting finite element model uses solid tetrahedral elements, anisotropic material constitutive laws, constraint equations to impose preload on bolts and contact conditions between parts [29,30], and it is solved in `MD-MSC Nastran`. The sizing of the bolted joint is performed considering an ultimate load condition and fatigue damage, according to international standards [10,31,32]. The results of the analysis are then fed back to the coarse aeroelastic level, as necessary.

2.3.2 Monodisciplinary structural optimization

The combined algorithm for optimizing the blade-tower structure is shown by the block diagram of Fig. 2. The aerodynamic shape is described by parameters $\boldsymbol{p}_a$ and it is fixed during the optimization. The DLC update and the structural optimization are performed

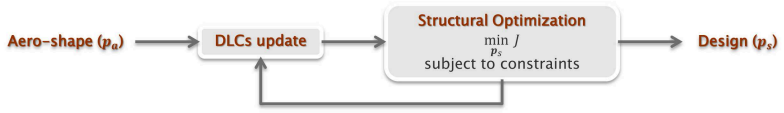

Figure 2 Monodisciplinary structural optimization with load freezing

iteratively, as shown by the diagram. The DLCs are estimated first, and then the optimization problem is solved on a guess structure, providing a new structural configuration denoted by parameters $\boldsymbol{p}_s$. The DLCs can be updated with the new layout, giving new conditions to the structural optimization problem. When the procedure converges, one has found the optimal structural design corresponding to the assigned aerodynamic configuration.

The minimization of the blade-tower cost can be expressed in algorithmic form as:

$$\textbf{Function } (\boldsymbol{p}_s^*, J^*) = \texttt{MinBladeTowerCost}(\boldsymbol{p}_a, \boldsymbol{p}_s, D, \boldsymbol{\Gamma}_s) : \tag{4a}$$
$$(\boldsymbol{E}) = \texttt{LoadEnvelope}(\boldsymbol{p}_a, \boldsymbol{p}_s, D), \tag{4b}$$
$$\textbf{do} \tag{4c}$$
$$(\boldsymbol{p}_{s1}, \boldsymbol{p}_{s2}) = \boldsymbol{p}_s, \tag{4d}$$
$$(\boldsymbol{p}_{s1}^*, J^*) = \texttt{MinCostBladeTowerFrozenLoads}(\boldsymbol{p}_a, \boldsymbol{p}_{s1}, D, \boldsymbol{E}, \boldsymbol{\Gamma}_s), \tag{4e}$$
$$(M) = \texttt{3DCADAndFEMeshGeneration}(\boldsymbol{p}_a, \boldsymbol{p}_{s1}^* \cup \boldsymbol{p}_{s2}, \boldsymbol{E}), \tag{4f}$$
$$(\boldsymbol{p}_{s2}^*, w_2^*, \boldsymbol{\Gamma}_s') = \texttt{3DFEAnalysis}(M, \boldsymbol{p}_{s2}, D, \boldsymbol{E}, \boldsymbol{\Gamma}_s), \tag{4g}$$
$$\boldsymbol{p}_s^* = \boldsymbol{p}_{s1}^* \cup \boldsymbol{p}_{s2}^*, \tag{4h}$$
$$(\boldsymbol{E}') = \texttt{LoadEnvelope}(\boldsymbol{p}_a, \boldsymbol{p}_s^*, D), \tag{4i}$$
$$\Delta p_{s1} = \|\boldsymbol{p}_{s1}^* - \boldsymbol{p}_{s1}\|, \quad \Delta J = \|J^* - J\|, \tag{4j}$$
$$\boldsymbol{p}_s = \boldsymbol{p}_s^*, \quad \boldsymbol{\Gamma}_s = \boldsymbol{\Gamma}_s', \tag{4k}$$
$$\textbf{while } (\Delta p_{s1} \geq \mathrm{tol}_{p_{s1}} \textbf{ and } \Delta J \geq \mathrm{tol}_J). \tag{4l}$$

The inputs of function `MinCostBladeTowerFrozenLoads` are the known parameters $\boldsymbol{p}_a$ describing the aerodynamic shape of the blade, the initial structural parameters $\boldsymbol{p}_s$, the data structure D defined in (3), and the load envelope $\boldsymbol{E}$, which is an array that contains for each verification section the maximum and minimum values of each internal stress resultant component throughout all DLCs. The same array contains as well the turbulent loads due to DLC 1.2 for fatigue damage computation [12]. The inputs further include a list of parameters $\boldsymbol{\Gamma}_s$ used to impose the design requirements, defined as

$$\boldsymbol{\Gamma}_s = \left(\boldsymbol{\sigma}_{\mathrm{adm}}, \boldsymbol{\epsilon}_{\mathrm{adm}}, \boldsymbol{\delta}_{\mathrm{tip}_{\mathrm{adm}}}, \boldsymbol{f}_{\mathrm{L}}, \boldsymbol{f}_{\mathrm{U}}, \ldots\right), \tag{5}$$

where $\boldsymbol{\sigma}_{\mathrm{adm}}$ and $\boldsymbol{\epsilon}_{\mathrm{adm}}$ are the admissible values for ultimate stress and strain, $\boldsymbol{\delta}_{\mathrm{tip}_{\mathrm{adm}}}$ is the allowable blade-tower clearance, and $[\boldsymbol{f}_{\mathrm{L}}, \boldsymbol{f}_{\mathrm{U}}]$ are vectors of upper and lower bounds for the desired placement of some chosen natural frequencies of the structure.

The outputs of the function are optimum values for the structural parameters $\boldsymbol{p}_s^*$ that produce a minimum cost J^*, where J is typically chosen as the mass or the ICC. The structural parameters are partitioned into primary $\boldsymbol{p}_{s1}$ and secondary $\boldsymbol{p}_{s2}$ parameters. The former

are the design variables used for parameterizing the cross sections (and that may include thickness of the external shell, spar caps, shear webs, and area of the leading and trailing edge reinforcements), while the latter include the shell core thickness that is pre-sized at the 2D level and then more accurately defined during the refinement cycle in (4f) and (4g).

The coarse-level constrained optimization (4e) takes the form:

$$\textbf{Function } (\boldsymbol{p}_s^*, J^*) = \texttt{MinCostBladeTowerFrozenLoads}(\boldsymbol{p}_a, \boldsymbol{p}_s, D, \boldsymbol{E}, \boldsymbol{\Gamma}_s): \tag{6a}$$

$$\boldsymbol{p}_s^* = \min_{\boldsymbol{p}_s} J(\boldsymbol{p}_s, D) \quad (\text{and } J^* = \arg\min_{\boldsymbol{p}_s} J), \tag{6b}$$

$$\text{s.t.:} \quad \boldsymbol{g}_s(\boldsymbol{p}_{s,b}, \boldsymbol{p}_{s,t}) \leq \boldsymbol{0}, \tag{6c}$$

$$\boldsymbol{\omega}_b(\boldsymbol{p}_{s,b}, D) \in [\boldsymbol{\omega}_L, \boldsymbol{\omega}_U], \tag{6d}$$

$$\boldsymbol{\sigma}_b(\boldsymbol{p}_{s,b}, \boldsymbol{E}, D) \leq \boldsymbol{\sigma}_{\text{adm}}, \tag{6e}$$

$$\boldsymbol{\epsilon}_b(\boldsymbol{p}_{s,b}, \boldsymbol{E}, D) \leq \boldsymbol{\epsilon}_{\text{adm}}, \tag{6f}$$

$$\boldsymbol{d}_b(\boldsymbol{p}_{s,b}, \boldsymbol{E}, D) \leq \boldsymbol{1}, \tag{6g}$$

$$\boldsymbol{\delta}_{\text{tip}_{\text{max}}}(\boldsymbol{p}_{s,b}, \boldsymbol{p}_{s,t}, \boldsymbol{E}, D) \leq \boldsymbol{\delta}_{\text{tip}_{\text{adm}}}, \tag{6h}$$

$$\boldsymbol{\omega}_t(\boldsymbol{p}_{s,t}, D) \in [\boldsymbol{\omega}_L, \boldsymbol{\omega}_U], \tag{6i}$$

$$\boldsymbol{\sigma}_t(\boldsymbol{p}_{s,t}, \boldsymbol{E}, D) \leq \boldsymbol{\sigma}_{\text{adm}}, \tag{6j}$$

$$\boldsymbol{d}_t(\boldsymbol{p}_{s,t}, \boldsymbol{E}, D) \leq \boldsymbol{1}. \tag{6k}$$

The primary structural variables $\boldsymbol{p}_{1s}$ are divided into the variables pertaining to the blade and those describing the tower, each group being identified by the subscript b and t, respectively. The same notation is applied to the set of design requirements expressed by inequalities (6c–6k), which have the following meaning:

- (6c): manufacturing, technological and geometrical constraints, as for example limits on the cone angle of the tower segments or to the span-wise ply tapering rates.
- (6d,6i): frequency placement constraints, to avoid resonant conditions by placing significant natural frequencies within a desired interval $[\boldsymbol{f}_L, \boldsymbol{f}_U]$. For example, this could be a requirement for the first flap blade eigenfrequency to lie above the three-per-rev at rated rotor speed, or for a suitable gap to exist between two consecutive blade frequencies. If the tower is considered, the first fore-aft and side-side frequencies could be located above (for a stiff design) or below (for a soft design) the one-per-rev at rated rotor speed.
- (6e, 6f, 6j): sufficient structural strength is obtained for the blade by imposing bounds on stress and strain components $\boldsymbol{\sigma}$ and $\boldsymbol{\epsilon}$, respectively, at a selected number of points on selected verification cross sections, according to [9, 10]. Von Mises stresses are considered for the tower, following Ref. [33].
- (6g, 6k): bounds on fatigue damage according to Ref. [9]. First, a fatigue damage index d_{σ_r} due to a single stress component is computed at preselected points on verification sections according to Ref. [10]. Then a multi-axial damage index is defined in agreement with Ref. [34, 35] as:

$$d_b = d_{\sigma_1}^{2/m} + d_{\sigma_1}^{2/m} - (d_{\sigma_1} d_{\sigma_2})^{1/m} + d_{\sigma_6}^{2/m}, \tag{7}$$

where m is the inverse slope of the Wöhler curve and the longitudinal, transverse and shear stress components are identified by indices 1, 2 and 6 respectively. The longitudinal and transverse stresses are perpendicular and tangent to the blade cross-section,

while the shear stress component lies in the plane of the cross-section. For the tower, the fatigue constraint implies the computation of the d_t index as indicated in Ref. [31]:

$$d_t = \left(\frac{\gamma_{Ff} \Delta\sigma_{E,2}}{\Delta\sigma_c / \gamma_{Mf}} \right)^3 + \left(\frac{\gamma_{Ff} \Delta\tau_{E,2}}{\Delta\tau_c / \gamma_{Mf}} \right)^5 , \tag{8}$$

where $\Delta\sigma_c$ and $\Delta\tau_c$ are reference values of fatigue strength, $\Delta\sigma_{E,2}$ and $\Delta\tau_{E,2}$ are equivalent constant amplitude stress ranges related to 2 million cycles, while γ_{Ff} and γ_{Mf} are safety factors. The damage indices for all verification points are stacked in vectors, $\boldsymbol{d}_b$ and $\boldsymbol{d}_t$, and they are all then bounded to unity.

– (6h): constraint to ensure blade-tower clearance for strike-free operation throughout all considered DLCs.

A refinement analysis (4g) can be applied to the solution obtained at the coarse aeroelastic level, by using 3D FEM models. To this end, all design constraints are recalculated, and the bounds at the aeroelastic level are updated based on the fine-level results, as explained in Ref. [12].

2.4 Limits of direct application of monodisciplinary aerodynamic and structural optimizations

Given the monodisciplinary optimization algorithms described in §2.2 and §2.3, the simplest possible approach to an aero-structural optimization of the rotor would consist in performing first the aerodynamic optimization, followed by the structural one. However, this method may produce sub-optimal design solutions, as well known to blade designers and further illustrated here by means of a simple example.

We consider as a baseline solution the DTU 10 MW RWT (Reference Wind Turbine) [36], whose configuration is, as all properly designed blades, a tradeoff between aerodynamic and structural considerations.

At first, the baseline blade was re-optimized from a purely aerodynamic point of view. To this end, the aerodynamic optimization was run by using as design variables both chord and twist parameters, while keeping the maximum chord constant and equal to the one of the reference blade. The aerodynamic optimum, as shown in Fig. 3(a), has a significant lower rotor solidity than the baseline blade, while only minor modifications affect the twist distribution. In fact, the optimization problem expressed in Eq. (1) tends to favor low values of rotor solidity, this way achieving a higher C_P at a higher λ, while limiting the extent of region II$^1/_2$.

However, given that the airfoils are not allowed to change, smaller chords also imply smaller thicknesses. This behavior is related to the constrained airfoil per-cent thickness that is implicitly defined when a specific airfoil series is selected. This means that bulkier structural elements are required in order to meet the stiffness requirements placed on the blade by the first flap frequency and tower clearance constraints. This is clearly illustrated by Fig. 3(b), which shows a dramatic increase in thickness of the spar cap. Therefore, the outcome of this simple optimization approach is a design of high aerodynamic efficiency, and hence high AEP, but also of very low structural efficiency, and hence of high mass. The CoE of the resulting blade is indeed higher than the one of the baseline blade, with an increase in this case of 2.6%.

Although this situation is well known and appreciated by most, it should be remarked that, in the absence of a true integrated optimization approach, there is not a *constructive*

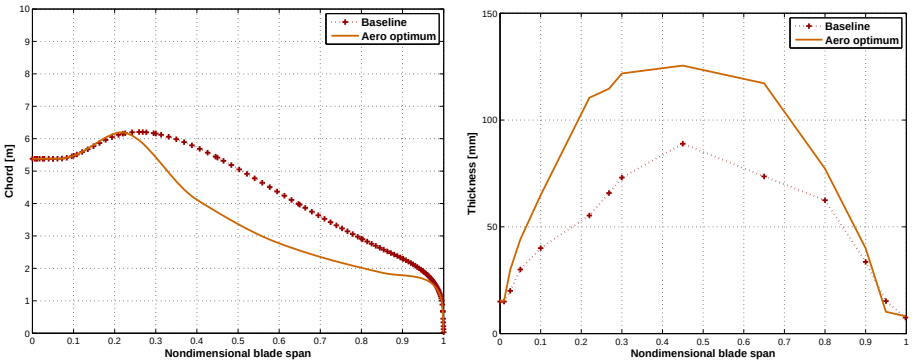

(a) Chord distribution comparison (b) Spar cap thickness distribution comparison

Figure 3 Results from sequential aerodynamic and structural optimizations

way to address this problem. Hence, it is difficult to make good use of the results shown above to find an improved solution. One might want to limit the decrease of solidity to try to counteract its negative effects on blade weight, but it is not clear how one could actually chose the optimal solidity value without embarking in a lengthy manual iteration.

Even more importantly, one should also realize that there are other more subtle couplings between the aero and structural solutions, which are even more difficult to account for. For example, although by decreasing the chord one decreases the thickness (which in turn negatively affects weight, as seen above), by doing so one also decreases the length of the skin panels in the chordwise direction. All the rest being the same, this increases the critical buckling load of the panels, which means that core thickness can be lowered, thereby reducing weight. Therefore, this example shows that the same change of an aerodynamic characteristic of the blade (in this case, solidity), might have opposing effects on weight, because of different effects on the sizing of its various structural members.

3 Aero-structural optimization algorithms

Some of the difficulties of designing rotor blades that were pointed out above can be alleviated by using integrated aero-structural procedures, where the aerodynamic and structural characteristics are considered together within one unique design process. The integration of the two disciplines should in fact allow one to define solutions of best compromise, according to a chosen criterion expressed by a selected figure of merit. Algorithms are described in the present chapter that try to achieve this goal by using different formulations, realizing different tradeoffs among complexity, computational cost and robustness. Three methods are considered: the Pre-Assumed Aerodynamic Shapes (PAAS) approach is presented in §3.1, the External Aerodynamic/Internal Structure (EAIS) approach in §3.2, while the Monolithic with Load Updating (MLU) approach is finally described in §3.3.

3.1 PAAS approach

The simplest possible aero-structural approach consists in first generating a parametric family of aerodynamic shapes, and then for each family member computing the associated opti-

mal structural configuration and the associated CoE. Next, a response surface can be used to interpolate the CoE in terms of the aerodynamic parametrization. Finally, the aerodynamic configuration corresponding to the minimum CoE can be readily computed on the response surface. Once this is found, a structural optimization performed on that aerodynamic shape yields the optimal aero-structural design. A conceptual depiction of the of the PAAS algorithm, first described in Ref. [2], is given by the block diagram shown in Fig. 4.

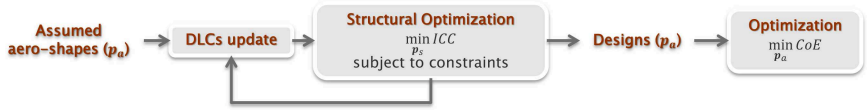

Figure 4 Block diagram of the PAAS optimization

The parameterization of the family of aerodynamic shapes is made by choosing a matrix $\boldsymbol{f}$ that includes predefined sets of constraints (1c) for the aerodynamic optimization. For example, as used later on in this work, such constraints may force the design of aerodynamic shapes with given pre-assumed values of the solidity, although other choices are clearly possible. The PAAS algorithm can be expressed in algorithmic form as follows:

$$\textbf{Function } (\boldsymbol{p}_a^*, \boldsymbol{p}_s^*, \boldsymbol{f}^*, CoE^*) = \texttt{PAASOptimization}(\boldsymbol{p}_a, \boldsymbol{p}_s, D, \boldsymbol{\Gamma}_s, \boldsymbol{f}): \tag{9a}$$

$$\textbf{for } i = 1:n \tag{9b}$$

$$(\boldsymbol{p}_{a_i}^*, P_{y_i}^*) = \texttt{MaxAEP}(\boldsymbol{p}_a, \boldsymbol{p}_s, D) \quad \text{with} \quad \boldsymbol{g}_a = \boldsymbol{f}_i, \tag{9c}$$

$$(\boldsymbol{p}_{s_i}^*, ICC_i^*) = \texttt{MinBladeCost}(\boldsymbol{p}_{a_i}^*, \boldsymbol{p}_s, D, \boldsymbol{\Gamma}_s), \tag{9d}$$

$$\textbf{end} \tag{9e}$$

$$(\boldsymbol{f}^*) = \texttt{OptimumAerodynamicShape}(\boldsymbol{ICC}^*, \boldsymbol{f}), \tag{9f}$$

$$(\boldsymbol{p}_a^*, P_y^*) = \texttt{MaxAEP}(\boldsymbol{p}_a, \boldsymbol{p}_s, D) \quad \text{with} \quad \boldsymbol{g}_a = \boldsymbol{f}^*, \tag{9g}$$

$$(\boldsymbol{p}_s^*, CoE^*) = \texttt{MinBladeCost}(\boldsymbol{p}_a^*, \boldsymbol{p}_s, D, \boldsymbol{\Gamma}_s). \tag{9h}$$

The loop generates a family of optimal aerodynamic shapes, by solving the monodisciplinary optimization expressed by (9c). This aerodynamic optimization function, defined in (1), has different constraints $\boldsymbol{g}_a = \boldsymbol{f}_i$ in (1c) for each index i, leading to blades characterized by different values of the chosen indexing parameters. Next, for each aerodynamic shape a monodisciplinary structural optimization is performed by (9d), subjected to its relevant design constraints, as previously discussed. Once the loop is completed, a family of optimal aerodynamic shapes has been generated together with their associated optimal structural sizings. Such discrete family is then interpolated by a response surface by function (9f), which readily yields the optimal set of constraints $\boldsymbol{f}^*$ that correspond to the minimum of the figure of merit ICC*. The aerodynamic shape corresponding to the optimal indexing parameters is then readily computed by (9g), followed by its structural sizing in (9h), therefore completing the problem.

The method is simple and robust: in fact, it relies exclusively on the ability to perform monodisciplinary optimizations. However, the method is also clearly limited, as the true

optimal solution can only be obtained if the family of aerodynamic shapes is chosen such as to contain it. Since the possible shapes that can be generated is limited by the choice of the family parameterization, the solution produced by this method will in general be suboptimal. Therefore, the method somewhat relies on the ability and knowledge of the user, and in the choices that are made for the indexing parameters.

Although the method has shown to work quite well in practice in a number of application, as also shown later on, the desire for more automated methods is clearly evident.

3.2 EAIS approach

To enable a true aero-structural optimization, thereby avoiding the limits of the PAAS algorithm, the new EAIS approach was developed. The two are somewhat similar, but for a crucial difference. In fact, in the EAIS case the choice of the aerodynamic parameters $\boldsymbol{p}_a$ is not left to the user, a major limitation, but it is handled by an external optimization loop. Scope of this loop is to explore the design space, proposing new aerodynamic solutions; for each, the algorithm evaluates the AEP and performs a structural sizing as previously explained, thereby allowing for the evaluation of a performance index, chosen here as the CoE. The exploration, which can in principle be conducted by a variety of different optimization methods, is terminated once an optimal constraint-satisfying solution is found. The overall algorithm is depicted in block diagram form in Fig. 5.

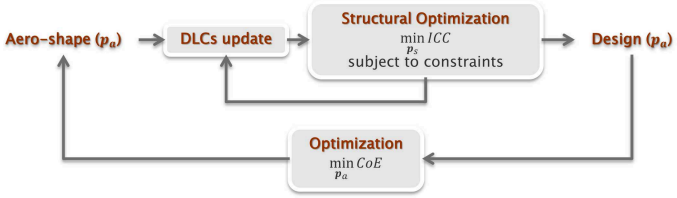

Figure 5 Block diagram of the EAIS optimization

The EAIS algorithm can be expressed in algorithmic form as follows:

$$\textbf{Function } (\boldsymbol{p}^*_{a,c}, \boldsymbol{p}^*_{a,t}, \boldsymbol{p}^*_s, CoE^*) = \texttt{EAISOptimization}(\boldsymbol{p}_a, \boldsymbol{p}_s, D, \boldsymbol{\Gamma}_s): \tag{10a}$$

$$\textbf{do} \tag{10b}$$

$$(\boldsymbol{p}^*_{a,c}) = \texttt{ChordGuess}(\boldsymbol{p}_{a,c}, CoE), \tag{10c}$$

$$(\boldsymbol{p}^*_{a,t}, \boldsymbol{p}^*_s, CoE^*) = \texttt{EAISCostFunction}(\boldsymbol{p}^*_{a,c}, \boldsymbol{p}_{a,t}, \boldsymbol{p}_s, D, \Gamma_s), \tag{10d}$$

$$\Delta p_{a,c} = \left\| \boldsymbol{p}^*_{a,c} - \boldsymbol{p}_{a,c} \right\|, \quad \Delta CoE = \left\| CoE^* - CoE \right\|, \tag{10e}$$

$$\boldsymbol{p}_{a,c} = \boldsymbol{p}^*_{a,c}, \quad CoE = CoE^*, \tag{10f}$$

$$\textbf{while } (\Delta p_{a,c} \geq \text{tol}_{p_{a,c}} \textbf{ and } \Delta CoE \geq \text{tol}_{CoE}). \tag{10g}$$

In the present implementation of the algorithm, the aerodynamic design parameters $\boldsymbol{p}_a$ are divided into chord and twist variables, noted $\boldsymbol{p}_{a,c}$ and $\boldsymbol{p}_{a,t}$, respectively. This is necessary to improve robustness and ease convergence, because of the typically small sensitivity of the

CoE with respect to the blade twist distribution. Therefore, the external aerodynamic optimization loop enclosed between (10b) and (10g) only manages the chord variables, while the twist variables are treated separately within the loop.

At first, a new planform shape of the blade is proposed by function `ChordGuess` in Eq. (10c). This function includes constraints in the form $\boldsymbol{g}_a(\boldsymbol{p}_{a,c}) \leq \boldsymbol{0}$ to express condition on the geometry of the chord distribution. This step is currently performed with the `patternsearch` algorithm of the MATLAB Global Optimization Toolbox [21]. Function `patternsearch` was chosen because it offers the ability to solve non-linear constrained optimization problems without requiring continuity and differentiability of the cost function, although other choices are clearly possible.

Next, the `EAISCostFunction` of Eq. (10d) completes the design, by finding the associated twist distribution and structural sizing, in turn enabling the evaluation of the CoE for this particular solution. This part of the process can be expressed in algorithmic form as follows:

$$\textbf{Function } (\boldsymbol{p}^*_{a,t}, \boldsymbol{p}^*_s, CoE^*) = \texttt{EAISCostFunction}(\boldsymbol{p}^*_{a,c}, \boldsymbol{p}_{a,t}, \boldsymbol{p}_s, D, \Gamma_s) : \tag{11a}$$

$$(\boldsymbol{p}^*_{a,t}) = \texttt{TwistOptMaxCp}(\boldsymbol{p}^*_{a,c}, \boldsymbol{p}_{a,t}, \boldsymbol{p}_s, D), \tag{11b}$$

$$\boldsymbol{p}^*_a = \boldsymbol{p}^*_{a,c} \cup \boldsymbol{p}^*_{a,t}, \tag{11c}$$

$$(\boldsymbol{p}^*_s, ICC^*) = \texttt{MinBladeCost}(\boldsymbol{p}^*_a, \boldsymbol{p}_s, D, \Gamma_s). \tag{11d}$$

As previously stated, in the EAIS optimization approach the design of the twist distribution becomes a nested and isolated problem that is solved before the structural sizing. This is accomplished by function `TwistOptMaxCp` in Eq. (11b), where the twist is optimized to maximize C_P while keeping the chord distribution fixed; possible geometric conditions on twist are expressed in the form $\boldsymbol{g}_a(\boldsymbol{p}_{a,t}) \leq \boldsymbol{0}$ and appended as constraints.

For each distribution of chord and twist corresponding to $\boldsymbol{p}^*_{a,c}$ and $\boldsymbol{p}^*_{a,t}$, the constrained structural optimization is then run to minimize the blade figure of merit in (11d). On the resulting complete blade design, the overall merit function CoE is evaluated, and the whole process is repeated until an optimal solution is found.

Compared to the PAAS method, the EAIS approach offers a fully automated procedure that, in principle, has the ability to more completely explore the solution space. In fact, it does not rely on a-priori choices of the aerodynamic shape of the blade, and it contains a mechanism to correctly couple not only the effects of aerodynamic choices to the structural design, but also to feed back to the aerodynamic design the results of the structural sizing. These desirable characteristics typically come at the price of a higher computational cost with respect to the PAAS approach.

3.3 MLU approach

The MLU approach merges the aerodynamic and structural design of rotor blades in a single optimization problem. Differently from the previous PAAS and EAIS approaches, in this method the structural and aerodynamic parameters are handled together within the same optimization procedure. Conceptually, the proposed approach is therefore an extension of the structural optimization reported in §2.3, with the addition of the aerodynamic design parameters. However, a key difference exists between the present approach and the structural optimization one: while in the former one can temporarily neglect variations in the loads

when the structural parameters are adjusted by the optimizer (variations that are then duly taken into account by the external load update, cf. Fig. 2), in the latter a technique is needed to estimate the effects that changes in the aerodynamic parameters have on loads. Clearly, a rigorous update could be made by simply recomputing all DLCs, but this would come at the price of a prohibitive computational cost. The solution developed here is shown in Fig. 6 in block diagram form: within the optimization block an approximate and fast update of the loads is performed, while accuracy is then regained by the external update of the DLCs. Even in this case, as for the monodisciplinary structural optimization, experience has shown that in general a couple of iterations are sufficient for achieving convergence.

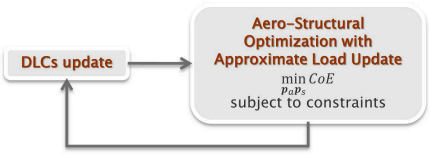

Figure 6 Block diagram of the MLU optimization

The algorithmic form of the MLU optimization is as follows:

$$\textbf{Function } (\boldsymbol{p}_a^*, \boldsymbol{p}_s^*, CoE^*) = \texttt{MLUOptimization}(\boldsymbol{p}_a, \boldsymbol{p}_s, D, \boldsymbol{\Gamma}_s) : \tag{12a}$$
$$(\boldsymbol{E}) = \texttt{LoadEnvelope}(\boldsymbol{p}_a, \boldsymbol{p}_s, D), \tag{12b}$$
$$\textbf{do} \tag{12c}$$
$$(\boldsymbol{p}_{s1}, \boldsymbol{p}_{s2}) = \boldsymbol{p}_s, \tag{12d}$$
$$(\boldsymbol{p}_a^*, \boldsymbol{p}_{s1}^*, CoE^*) = \texttt{MinCostMLUApproach}(\boldsymbol{p}_a, \boldsymbol{p}_{s1}, D, \boldsymbol{E}, \boldsymbol{\Gamma}_s), \tag{12e}$$
$$(M) = \texttt{3DCADAndFEMeshGeneration}(\boldsymbol{p}_a^*, \boldsymbol{p}_{s1}^* \cup \boldsymbol{p}_{s2}, \boldsymbol{E}), \tag{12f}$$
$$(\boldsymbol{p}_{s2}^*, w_2^*, \Gamma_s') = \texttt{3DFEAnalysis}(M, \boldsymbol{p}_{s2}, D, \boldsymbol{E}, \boldsymbol{\Gamma}_s), \tag{12g}$$
$$\boldsymbol{p}_s^* = \boldsymbol{p}_{s1}^* \cup \boldsymbol{p}_{s2}^*, \tag{12h}$$
$$(\boldsymbol{E}') = \texttt{LoadEnvelope}(\boldsymbol{p}_a^*, \boldsymbol{p}_s^*, D), \tag{12i}$$
$$\Delta p_a = \|\boldsymbol{p}_a^* - \boldsymbol{p}_a\|, \quad \Delta p_{s1} = \|\boldsymbol{p}_{s1}^* - \boldsymbol{p}_{s1}\|, \quad \Delta CoE = \|CoE^* - CoE\|, \tag{12j}$$
$$\boldsymbol{p}_a = \boldsymbol{p}_a^*, \quad \boldsymbol{p}_s = \boldsymbol{p}_s^*, \quad \boldsymbol{\Gamma}_s = \boldsymbol{\Gamma}_s', \tag{12k}$$
$$\textbf{while } (\Delta p_a \geq \text{tol}_{p_a} \textbf{ and } \Delta p_{s1} \geq \text{tol}_{p_{s1}} \textbf{ and } \Delta CoE \geq \text{tol}_{CoE}). \tag{12l}$$

The algorithm is very similar to the purely structural optimization expressed in (4), except that in this case both the aerodynamic and structural parameters are handled together. The actual monolithic optimization is performed in (12e), which is implemented as follows:

$$\textbf{Function } (\boldsymbol{p}_a^*, \boldsymbol{p}_s^*, CoE^*) = \texttt{MinCostMLUApproach}(\boldsymbol{p}_a, \boldsymbol{p}_s, D, \boldsymbol{E}_0, \boldsymbol{\Gamma}_s): \tag{13a}$$

$$(\boldsymbol{p}_a^*, \boldsymbol{p}_s^*) = \min_{\boldsymbol{p}_a, \boldsymbol{p}_s} CoE(\boldsymbol{p}_a, \boldsymbol{p}_s, D) \quad (\text{and } CoE^* = \arg\min_{\boldsymbol{p}_a, \boldsymbol{p}_s} CoE), \tag{13b}$$

$$\text{s.t.:} \quad \boldsymbol{g}_a(\boldsymbol{p}_a) \leq \boldsymbol{0}, \tag{13c}$$

$$\boldsymbol{g}_s(\boldsymbol{p}_s) \leq \boldsymbol{0}, \tag{13d}$$

$$\boldsymbol{\omega}(\boldsymbol{p}_s, D) \in [\boldsymbol{\omega}_L, \boldsymbol{\omega}_U], \tag{13e}$$

$$\boldsymbol{\sigma}(\boldsymbol{p}_s, \boldsymbol{E}, D) \leq \boldsymbol{\sigma}_{\text{adm}}, \tag{13f}$$

$$\boldsymbol{\epsilon}(\boldsymbol{p}_s, \boldsymbol{E}, D) \leq \boldsymbol{\epsilon}_{\text{adm}}, \tag{13g}$$

$$\boldsymbol{d}(\boldsymbol{p}_s, \boldsymbol{E}, D) \leq \boldsymbol{1}, \tag{13h}$$

$$\boldsymbol{\delta}_{\text{tip}_{\max}}(\boldsymbol{p}_s, \boldsymbol{E}, D) \leq \boldsymbol{\delta}_{\text{tip}_{\text{adm}}}. \tag{13i}$$

$$\text{where} \quad (\boldsymbol{p}_{a,t}^*) = \texttt{TwistOptMaxCp}(\boldsymbol{p}_{a,c}^*, \boldsymbol{p}_{a,t}, \boldsymbol{p}_s, D), \tag{13j}$$

$$\boldsymbol{p}_a = \boldsymbol{p}_{a,c} \cup \boldsymbol{p}_{a,t}^*, \tag{13k}$$

$$(\boldsymbol{E}) = \texttt{ApproximateLoadUpdate}(\boldsymbol{p}_a, \boldsymbol{E}_0). \tag{13l}$$

The figure of merit is the CoE, while the set of constraints is the union between the ones of algorithm (1) and those of (6), whose meaning was given in §2.2 and §2.3, respectively. As the optimization is subjected to a possibly large number of constraints, many of which are typically active at convergence, here again the SQP approach is used for solving the problem. Since the analysis environment is complex and it implies the interaction of multiple simulation tools, the only reasonably simple way to estimate gradients is by finite differences.

As for the EAIS approach, even here the twist of the blade is treated separately from the chord, to improve convergence in the face of a low sensitivity of the cost function to twist changes. This is achieved here by function `TwistOptMaxCp`, which computes $\boldsymbol{p}_{a,t}$ for any chord distribution $\boldsymbol{p}_{a,c}$, as explained in §3.2.

The core of the procedure is expressed by (13l), which implements a method for the approximate update of the load envelope $\boldsymbol{E}$ without actually re-running the relevant DLCs. Within the optimization, whenever the aerodynamic parameters $\boldsymbol{p}_a$ are modified, function `ApproximateLoadUpdate` is called to estimate variations to the loads $\boldsymbol{E}_0$ computed at the last run of all DLCs.

Different approximate update procedures are applied to the ultimate and fatigue loads. Regarding the former, the update is simply performed by scaling the aerodynamic loads by changes in the chord, as shown in Fig. 7. In fact, neglecting changes in the inflow, according to strip theory a change in chord will produce a proportional change in aerodynamic forces. The effects of changes in twist are neglected. The gravitational and inertial contributions to ultimate loads are on the other hand exactly updated based on the current values of the structural design parameters.

For the approximate update of the fatigue damage a different approach is considered. In fact, fatigue damage depends on the dynamic response of the machine and the ensuing loads. Therefore, a simple scaling of the aerodynamic loads, as performed for the ultimate ones, is typically not accurate enough. The problem is solved here by using a coarse model of the wind turbine with a limited number of degrees of freedom, so as to enable the simulation of the necessary turbulent responses in limited time. Such model is not accurate enough to estimate the actual fatigue damage, but it is capable of capturing the sensitivity of fatigue damage to changes in the aerodynamic design parameters. The simplified model for fatigue

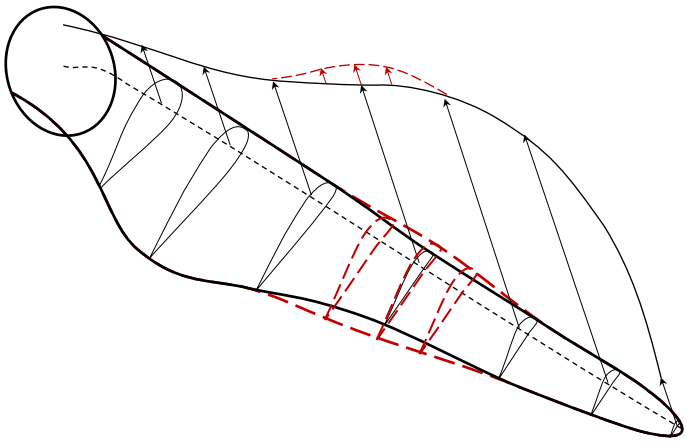

Figure 7 Update of the aerodynamic contribution to ultimate loads by chord scaling

assessment consists of one single flexible blade, the other blades being modeled as rigid bodies, while two prismatic joints with their associated stiffness characteristics are used to match the low frequency fore-aft and side-side behavior of the tower. Since the reduced model is capable of correctly estimating the damage trend, the fatigue damage index $\boldsymbol{d}$ is updated as follows:

$$\boldsymbol{d} = \boldsymbol{d}_0 + (\boldsymbol{d}_{SM} - \boldsymbol{d}_{SM,0}), \tag{14}$$

where $(\cdot)_{SM}$ refers to the simplified model, while $(\cdot)_0$ are values computed for the blade configuration when the DLCs were last run.

4 Applications and results

4.1 Definition of a baseline blade

The three aero-structural design methods described in this paper were applied to the DTU 10 MW RWT, which was chosen as a significant test case representing the next generation very large HAWTs. The DTU 10 MW RWT is a conceptual machine developed by Danmarks Tekniske Universitet (DTU), freely availably in the public domain for research purposes [36]. The main characteristics of the wind turbine are reported in Table 1, while a more complete description of the model and the criteria used for its design are given in Ref. [37].

The structural configuration of the blade is shown in Fig. 8, while Table 2 reports the spanwise extension of the structural components and their materials. The blade has a rather standard configuration, except perhaps for the presence of a third shear web towards the trailing edge extending over a good part of the blade span. Unidirectional fiberglass reinforcements are located at the leading edge (LE) and trailing edge (TE), while an additional reinforcement is superimposed to the external shell in the blade root region. Transversely isotropic laminae are assumed with mechanical properties reported in Table 3 [37]. The mechanical properties of the resulting laminates are computed by classical lamination theory.

Table 1 Main parameters of the DTU 10 MW RWT

Data	Value
Wind class	IEC 1A
Rated power	10 MW
Cut-in wind speed	4 m/s
Cut-out wind speed	25 m/s
Rotor diameter	178.3 m
Hub height	119.0 m

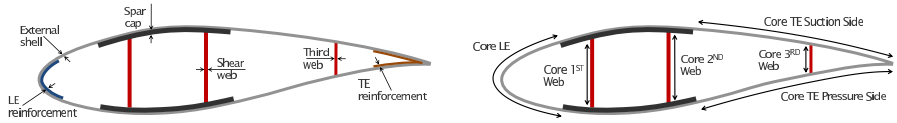

(a) Main structural components (b) Secondary core structures

Figure 8 Configuration of the blade section

Table 2 Extent of the structural components and their materials

Component	Starting section (% span)	Ending section (% span)	Material type
External shell	0	100	Stitched triaxial -45/0/+45 fiberglass
Spar caps	1	99.8	Unidirectional fiberglass
First and second shear webs	5	99.8	Stitched biaxial -45/+45 fiberglass
Third shear web	22	95	Stitched triaxial -45/0/+45 fiberglass
Trailing and leading edge reinforcements	10	95	Unidirectional fiberglass
Root reinforcement	0	45	Unidirectional fiberglass
External shell core	5	99.8	Balsa
Web core	5	99.8	Balsa

Table 3 Material properties

Material type	Longitudinal Young's modulus [MPa]	Transversal Young's modulus [MPa]	Shear modulus [MPa]
Stitched triaxial -45/0/+45 fiberglass	21790	14670	9413
Unidirectional fiberglass	41630	14930	5047
Stitched biaxial -45/+45 fiberglass	13920	13920	11500
Balsa	50	50	150

Before proceeding with the test of the aero-structural design algorithms, the RWT blade was subjected to a mono-disciplinary multi-level structural optimization performed using the current tools, in order to refine certain aspects of its design.

Namely, the nonstructural mass estimation was improved, by not only including the core (sized so as to ensure a buckling free state in all operating conditions) but also considering adhesive, resin uptake, bonding plies, lightening system and external paint. Furthermore, the blade root design was modified, by increasing the laminate thickness to accommodate bolted joints. The laminate sizing in the root region was verified by a detailed 3D FEM model of the pretensioned bolts.

At first, an analysis of the DLCs was made, to identify the dominating ones. Based on the results of this preliminary investigation, DLCs 1.1, 1.2, 1.3, 2.1, 2.3, 6.1, 6.2 and 6.3 [9] were identified as the design drivers, and were included in the optimization process. The DLCs list enumerates heterogeneous load cases that embrace power production in stochastic wind field with different turbulent intensities, idling conditions and fault simulations during wind gusts. The design included all features previously described, including constraints on blade-tower clearance, ultimate stress, ultimate strain and fatigue damage. Considering the blade-tower clearance, the pre-bend of the blade was modeled as an extra rotor cone angle equal to 2.15 deg. Design requirements were also applied to the blade modal properties, imposing a first blade flap frequency separation from the three-per-rev at rated rotor speed of at least 16%, as well as a gap between the first flap and lag frequencies of at least 10%. Additional geometric conditions on maximum thickness and tapering rates of the laminates were also included to translate manufacturing and technological constraints.

The structurally re-optimized blade obtained from the RWT is termed here and in the following “baseline”, as it will be used as the starting point for the subsequent analyses conducted with the proposed algorithms.

For the obtained baseline blade, the active (A) and non-active (N) constraints at convergence are reported in Table 4. The results indicate that blade-tower clearance and fatigue damage drive the design, while the requirements on ultimate load conditions and frequency placement are not active.

Table 4 Active and non-active structural constraints for the baseline solution

Stress/ strain	Frequency placement	Clearance	Fatigue
N	N	A	A { External shell from 22% to 65% span Shear web from 22% to 80% span Root reinforcement from 22% to 45% span

A comparison between the RWT and baseline blades is shown in Fig. 9. All quantities are plotted as functions of the non-dimensional blade span, that is null at the root and unitary at the tip.

Looking at Fig. 9(a), the baseline blade has a noticeable increase in the thickness of the external shell, with a subsequent noticeable weight increment in this part of the blade; this is due to the redesign performed to accommodate the root bolts. The same diagram shows also a reduction of the shell thickness in the outer part of the blade. This is compensated by an increase in the spar cap thickness, as shown in Fig. 9(b), driven by the blade-tower clearance requirement. This leads to a more efficient structure that minimizes the overall mass. A comparison between the original nonstructural mass distribution and the baseline

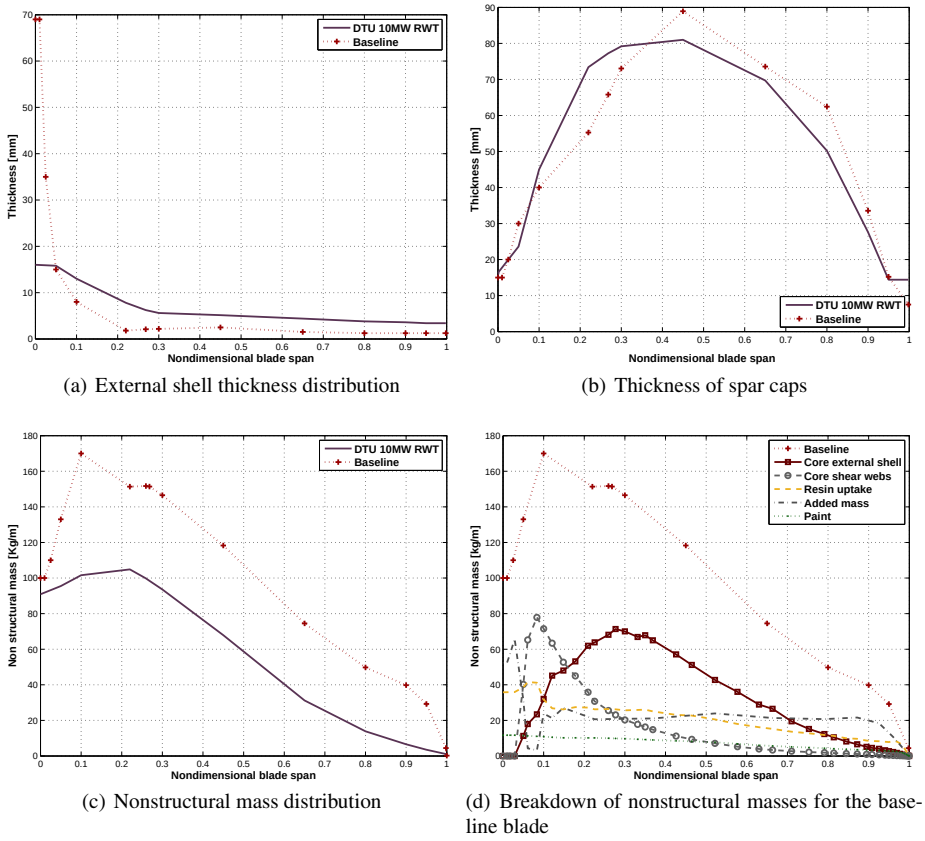

(a) External shell thickness distribution

(b) Thickness of spar caps

(c) Nonstructural mass distribution

(d) Breakdown of nonstructural masses for the baseline blade

Figure 9 Comparison between the RWT and baseline blade designs

one is shown in Fig. 9(c): the plot shows a noticeable increase with respect to the reference design, mainly due to the additional contributions considered here. A breakdown of the updated nonstructural masses is shown in Fig. 9(d), where the contributions of the adhesive applied during manufacturing, resin uptake, bonding plies and lightening system are all grouped together and labelled "added mass".

The structural optimization was conducted by multiple iterations between the coarse aeroservoelastic level and the fine 3D FEM level, until all constraints were satisfied also at the latter one. 3D FE analyses are performed by `MSC Nastran 2012`, using `CQUAD` plate elements, including transverse shear, membrane, bending and coupling between membrane and bending deformation. Different analyses are considered, including linear static load cases, linear buckling and modal analysis, aiming at a verification of the design requirements. An example of the 3D analysis is reported in Fig. 10, which shows the constraint on ultimate stresses at some critical verification sections along the blade span.

At the end of the optimization, the complete set of all DLCs was run again, to verify that none of the ones that were left out of the optimization process had in the meanwhile become design drivers.

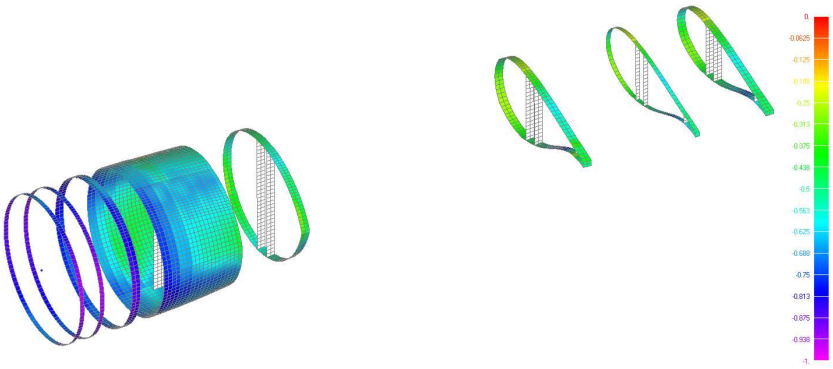

Figure 10 Constraint on normal stress for the converged baseline solution, showing that the condition is verified everywhere

The optimized baseline blade was then used as a starting guess and as a comparison for the proposed aero-structural optimization algorithms formulated earlier in this work, as described in the next section.

4.2 Aero-structural design performance comparison

Considering the baseline blade described in the previous section as the initial configuration, the proposed aero-structural optimization algorithms were then used for redesigning the blade. All three methods were used with the same identical design requirements and conditions, in order for the results to be directly comparable.

To allow for a more precise comparison of the three methods, especially in their ability to define aerodynamic shapes and associated structural sizings, the optimization of the baseline was made while keeping the rotor radius fixed, together with other macro-design parameters of the wind turbine, such as tower height, rated power, rotor uptilt and cone, and material properties. Therefore, the design parameters only included the blade chord and twist, and the structural sizes of spar caps, shear webs, skin, reinforcements and core. Given this restriction of the solution space, only limited changes in CoE are to be expected. A more general holistic resizing of this machine by the present design tools will be described in a forthcoming publication.

For the PAAS approach, a family of solutions was obtained for varying solidity σ. For each chosen σ, a constraint was also placed on the maximum chord $c_{\max}$, to avoid the appearance of shapes of excessive tapering. The $c_{\max}$ constraint was scaled linearly with σ. Aerodynamic optimizations were run for each of the parameters, followed by structural optimizations, the former with the goal of maximizing AEP and the latter of minimizing ICC. The results in terms of chord and twist distributions are shown in Fig. 11(a) and Fig. 11(b), respectively. Each design is identified by the label PAASi, where i goes from 1 to 5 and solidity assumes values from 4.0% to 6.5%. An interpolation using a cubic spline is then performed on the resulting CoEs of the five designs, on which the minimum cost is readily identified for σ equal to 5.32% and a corresponing $c_{\max}$ equal to 7.4 m. Assuming these values as constraints, a new AEP optimal aerodynamic shape is generated with these characteristics, followed by an optimal structural sizing for minimum ICC. The resulting aero-structural configuration, labelled simply PAAS in the following, is the result of this first

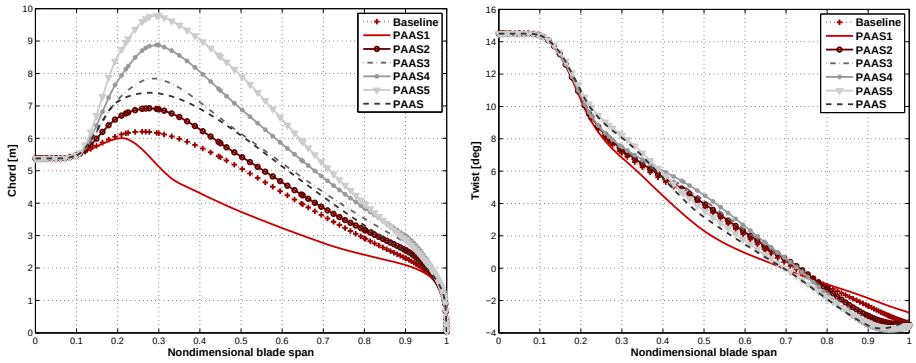

(a) Chord distribution for the PAAS family of AEP optimal solutions

(b) Twist distribution for the PAAS family of AEP optimal solutionss

Figure 11 PAAS approach: AEP optimal aerodynamic shapes parameterized in terms of rotor solidity

simple optimization method, and used for comparison with the other two more sophisticated approaches.

Next, the EAIS and MLU approaches were used to optimize the baseline configuration, under the same identical design requirements adopted for PAAS. The only difference was in this case that the aerodynamic shape was left free to evolve, without imposing constraints on solidity.

A comparison of some important characteristics of the solutions is reported in Fig. 12, in terms of percent variations from the baseline blade.

Figure 12(a) reports the results for the figure of merit. The largest reduction is obtained by the MLU approach, followed by the EAIS one. Examining the solidity in Fig. 12(b), it is evident that the σ values of the EAIS and MLU configurations are very close to the optimum of the PAAS approach, and all three methods essentially reach a very simular CoE. The minimum of CoE can be explained by looking at the AEP and blade mass diagrams reported in Fig. 12(c) and Fig. 12(d), respectively. As shown by the PAAS family of solutions, AEP tends to decrease for increasing solidity. On the other hand, mass exhibits a minimum for intermediate values of solidity. In fact, at low σ values, an increase of solidity leads to a higher structural efficiency and to a reduction of the mass of the blade. However, this is true only until buckling does not become an active constraint. At higher σ, the blade is characterized by large and thin panels, which are indeed prone to instability. The core thickness must then be increased to avoid buckling, causing an increase of nonstructural mass that in turn increases the blade total mass.

Although even the simple PAAS approach is able to identity these subtle tradeoffs, EAIS and MLU lead to slightly better results. This is due to their larger freedom in adjusting the shape of the blade, while PAAS is clearly limited by the choices made a priori when defining the assumed family of solutions. All resulting designs are however quite similar, and for all the active structural constraints include clearance, fatigue and buckling.

The aerodynamic solutions are shown in Fig. 13, while the thickness of the principal structural components are displayed in Fig. 14. The solutions in terms of chord distributions are all quite similar for the three methods. Twist on the other hand is different for the innermost part of the blade, while a better agreement among the solutions is obtained from approximatively 45% span to the blade tip. This small discrepancy is due to the different

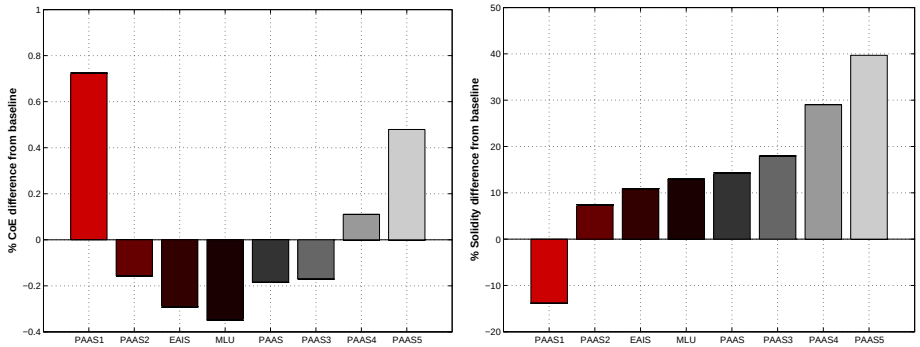

(a) CoE

(b) Solidity

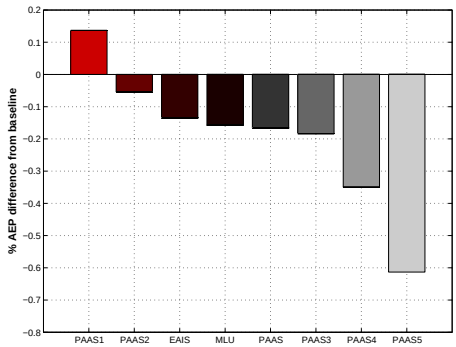

(c) AEP

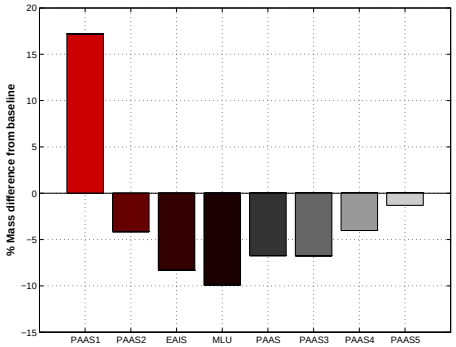

(d) Blade mass

Figure 12 Aero-structural algorithms: per cent change of some selected parameters with respect to the baseline configuration

ways the aerodynamic design parameters are handled by the various methods. In fact, in the PAAS approach chord and twist are optimized for maximum AEP for each of the family members, while in the EAIS and MLU approaches twist is computed so as to maximize the power coefficient while keeping the chord fixed. Due to this, the EAIS and MLU designs exhibit slightly higher power coefficients than PAAS, but the resulting differences in terms of AEP are negligible. Differences among solutions are even more negligible when evaluated in terms of CoE.

Looking at the structural parameters, a good agreement is reported in general among all methods.

Regarding the computational costs, a comparison among the three approaches is reported in Table 5. Figures are normalized with respect to the cost of the PAAS solution, which appears to be the least expensive. It should however be remarked that in this case to find a good optimal solution it was sufficient to generate a one-parameter family composed of only 5 members. In other cases, a more extensive multi-parameter approximation of the solution space might be necessary, which would increase the computational cost of this approach. The MLU method appears to be quite computationally efficient, with costs that are only marginally higher than PAAS. This however comes at the cost of a significantly higher complexity of the code, together with a somewhat reduced robustness due to the approxi-

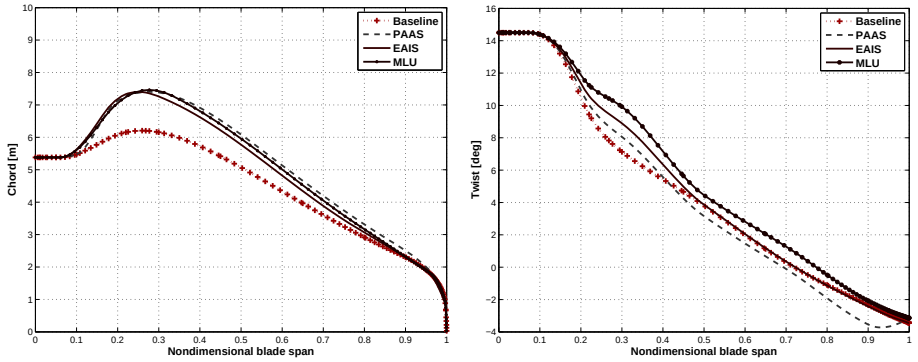

(a) Blade chord (b) Blade twist

Figure 13 Aero-structural algorithms: comparison of blade aerodynamic design parameters

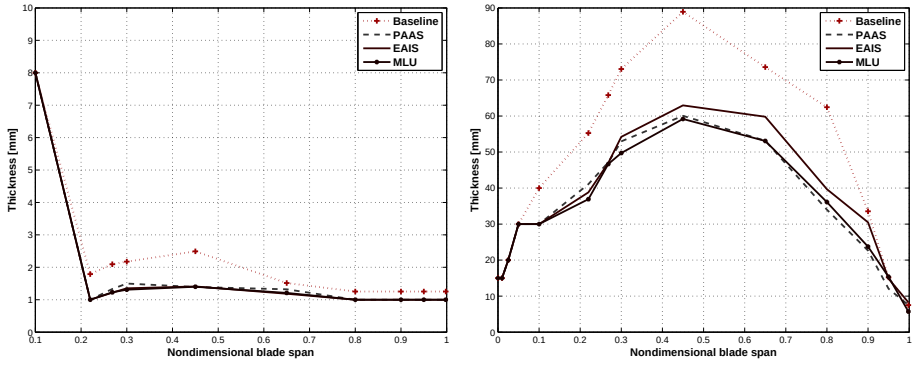

(a) External shell thickness distribution (b) Spar cap thickness distribution

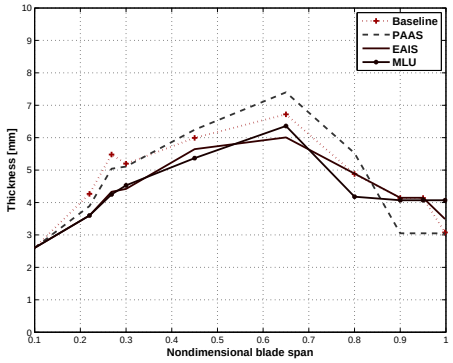

(c) Shear web thickness distribution

Figure 14 Aero-structural algorithms: comparison of blade structural design parameters

mations that form the basis of the load updates. The MLU approach appears to be the most expensive of the three in this case. However, its higher cost comes with a significant generality and robustness. As the cost is higher but still manageable, this method might be the one to choose for complex design problems.

Table 5 Relative computational costs for the aero-structural algorithms

Algorithm	PAAS	EAIS	MLU
Relative computational costs	1	3	1.25

5 Conclusions

Three aero-structural optimization algorithms were described in this paper for the design of wind turbines. The procedures are focused on the design of the rotor, and optionally of the tower. All approaches are based on the same high fidelity aeroservoelastic simulation environment that enables the evaluation of the necessary performance and response indicators by accounting for all fundamental physical effects in the various operating conditions prescribed by international standards.

The aerodynamic and structural characteristics of the wind turbine are parameterized by a set of optimization variables. Cost models are used for finding optimal tradeoffs among the design variables.

The algorithms that were presented herein differ significantly in the way they approach this complex multidisciplinary design problem:

- PAAS generates a population of aerodynamically optimal blades, each with its associated optimal structural sizing, the population being parameterized in terms of relevant aerodynamic quantities chosen by the analyst. Aerodynamic and structural optimizations are applied sequentially, sampling the solution domain. The best solution is obtained by interpolation of these resulting different designs. This approach is robust and it has a reduced computational cost, but it is limited by the ability of the user in defining an appropriate population that actually contains the optimal solution. In this sense, the method is limited by the experience and insight of the user.
- EAIS overcomes the limits of PAAS, by automating the aerodynamic parametrization of the model. An external optimization loop handles the aerodynamic variables, while an internal one generates an optimal structure for each aerodynamic configuration proposed by the external loop. The method is general and robust, but may imply a higher computational cost.
- MLU unifies the aerodynamic and the structural variables in a monolithic algorithm. To reduce cost, the sensitivity of the solution to changes in the aerodynamic variables is initially updated by simplified models, while an iterative procedure ensures accuracy, eliminating the approximations induced by the simplified updates. The algorithm is faster than EAIS, but more complicated and in general less robust than the other two.

The three proposed aero-structural design methods were applied to a conceptual 10 MW HAWT test case. All three methods converge to essentially the same solution, demonstrating that all are capable of solving the multidisciplinary optimization problem.

The results show that the aero-structural optimization of this particular wind turbine favors a rotor design with higher values of solidity and maximum chord than the initial baseline. This allows for a higher structural efficiency without significantly depressing the aerodynamic performance. Compared to the baseline configuration, the aero-structural optimum achieves a reduction of 9.41% of the blade mass with a reduction of AEP of 0.16%. This results in ICC savings of 0.57% and CoE savings of 0.33%. Although these are relatively small numbers, it should be remarked once again that the redesign of the blade was performed for a fixed value of the rotor radius (as well of many other design parameters of the wind turbine), an assumption that inherently limits the possible changes in ICC and CoE, irrespectively of the method used. A future publication will apply the proposed procedures to a more holistic redesign of the machine.

Efforts are also underway to improve the cost models, which play a crucial role here since they essentially drive the definition of the tradeoffs among the various disciplines and the many different requirements. The method of Ref. [38] is currently being implemented together with other detailed engineering estimates, with the goal of replacing as much as possible statistical extrapolations of costs based on historical data in favor of the detailed physical models that are used by the proposed design procedures. In fact, although cruder and hence faster wind turbine rotor design methods can be formulated, we believe that the level of detail implied by our proposed methods allows for a more exact assessment of the various contributing factors to cost.

Acknowledgement

The present work is partially supported at the Politecnico di Milano by the EU FP7 INNWIND project.

References

1. Ning N.S., Damiani R., Moriarty, P.J.: Objectives and constraints for wind turbine optimization, 51st AIAA Conference, January 2013
2. Bottasso C.L., Campagnolo F., Croce A.: Multi-disciplinary constrained optimization of wind turbines. Multibody Syst. Dyn. DOI: 10.1007/s11044-011-9271-x (2011)
3. Bottasso C.L., Croce A., Sartori L., Grasso, F.: Free-form design of rotor blades. Proceedings of the Science of Making Torque from Wind, Copenhagen, June 2014
4. Maki K., Sbragio R., Vlahopoulos N.: System design of a wind turbine using a multi-level optimization. Renewable Energy, **43**, 101-110 DOI: 10.1016/j.renene.2011.11.027 (2012)
5. Vesel Jr. R.W., McNamara J.J.: Performance enhancement and load reduction of a 5 MW wind turbine blade. Renewable Energy, **66**, 391-401 DOI: 10.1016/j.renene.2013.12.019 (2014)
6. Kenway G., Martins J.R.R.A.: Aerostructural shape optimization of wind turbine blades considering site-specific winds. 12th AIAA/ISSMO Multidisciplinary Analysis and Optimization Conference, September 10th-12th, DOI: 10.2514/6.2008-6025 (2008)
7. Ashuri T., Zaaijer M.B., Martins J.R.R.A., van Bussel G.J.W., van Kuik G.A.M.: Multidisciplinary design optimization of offshore wind turbines for minimum levelized cost of energy. Renewable Energy, **68**, 893–905 10.1016/j.renene.2014.02.045 (2014)
8. Fischer G.R., Kipouros T., Savill A.M.: Multi-objective optimization of horizontal axis wind turbine structure and energy production using aerofoil and blade properties as design variables. Renewable Energy, **62**, 506-515, 10.1016/j.renene.2013.08.009 (2014)
9. Wind Turbines — Part 1: Design Requirements, Ed. 3. International Standard IEC 61400-1 (2005)
10. Guideline for the Certification of Wind Turbines, Ed. 2010. Germanischer Lloyd Industrial Services GmbH, Renewables Certification, Brooktorkai 10, 20457 Hamburg, Germany (2010)
11. Bottasso C.L., Croce A., Savini B., Sirchi W., Trainelli L.: Aero-servo-elastic modeling and control of wind turbines using finite-element multibody procedures. Multibody Syst. Dyn. DOI:10.1007/s11044-006-9027-1 (2006)

12. Bottasso C.L., Campagnolo F., Croce A., Dilli S., Gualdoni F., Nielsen M.B.: Structural optimization of wind turbine rotor blades by multi-level sectional/multibody/3D-FEM analysis. Multibody Syst. Dyn. DOI:10.1007/s11044-013-9394-3 (2014)
13. Bottasso C.L., Croce A.: `Cp-Lambda`: User's Manual. Dipartimento di Scienze e Tecnologie Aerospaziali, Politecnico di Milano (2006–2014)
14. Bauchau O.A., Epple A., Bottasso C.L.: Scaling of constraints and augmented Lagrangian formulations in multibody dynamics simulations, Journal of Computational and Nonlinear Dynamics, Vol. 4, N. 2, DOI:10.1115/1.3079826 (2009)
15. Bauchau O.A.: Flexible Multibody Dynamics. Springer, Solid Mechanics and its Applications, Vol. 176 (2011)
16. Bauchau O.A., Bottasso C.L., Trainelli L.: Robust integration schemes for flexible multibody systems. Comput. Meth. Appl. Mech. Eng. **192**, 395–420 (2003)
17. Hansen M.O.L.: Aerodynamics of Wind Turbines. Earthscan, 2nd Edition (2008)
18. Pitt D.M., Peters D.A.: Theoretical prediction of dynamic inflow derivatives. Vertica **5**, 2134 (1981)
19. Peters D.A., He C.J.: Finite state induced flow models — Part II: Three-dimensional rotor disk. J. Airc. 32, 323333, DOI:10.2514/3.46719 (1995)
20. NWTC Computer-Aided Engineering Tools: TurbSim by Neil Kelley, Bonnie Jonkman. http://wind.nrel.gov/designcodes/preprocessors/turbsim/.
21. `Matlab`. The MathWorks Inc., 3 Apple Hill Drive, Natick, MA 01760-2098, USA, `www.mathworks.com`
22. Gill P.E., Murray W.,Wright M.H.: Pratical Optimization. Academic Press, (1981)
23. Bottasso C.L., Croce A., Nam Y., Riboldi C.E.D.: Power curve tracking in the presence of a tip speed constraint. Renew. Energy. **40**, 1–12 DOI: 10.1016/j.renene.2011.07.045 (2012)
24. Giavotto V., Borri M., Mantegazza P., Ghiringhelli G.: Anisotropic beam theory and applications. Comput. Struct. **16**, 403–413 (1983)
25. Fingersh L., Hand M., Laxson A.: Wind turbine design cost and scaling model. Technical Report NREL/TP-500-40566 (2006)
26. Lindenburg C., de Winkel G.D.: Buckling load prediction tools for rotor blades. ECN-C-05-103, (2005)
27. `HyperMesh`. Altair Engineering, 1820 Big River Rd, Troy, MI 48082, USA, `www.altair.com`
28. `Tcl` DeveloperXchange: `www.tcl.tk`
29. `MD/MSC NASTRAN` 2010 Quick Reference Guide. MSC Software (2010)
30. `MD/MSC NASTRAN` 2011 MD Demonstration Problems. MSC Software (2011)
31. European Standard Eurocode 3: Design of Steel Structures — Part 1–9: Fatigue, Ed. 2005. European Committee for Standardization, rue de Stassart, 36, B-1050 Brussels
32. VDI 2230 RICHTLINIEN: Systematic calculation of high duty bolted joints, February 2003, Verein Deutscher Ingenieure, Düsseldorf
33. European Standard Eurocode 3: Design of Steel Structures — Part 1–6: Strength and Stability of Shell Structures, Ed. 2007. European Committee for Standardization, rue de Stassart, 36, B-1050 Brussels
34. Philippidis T.P., Vassilopoulos A.P.: Complex stress state effect on fatigue life of GRP laminates. Part I, experimental. Int. J. Fatigue. **24**, 813–823 (2002)
35. Philippidis T.P., Vassilopoulos A.P.: Complex stress state effect on fatigue life of GRP laminates. Part II, theoretical formulation. Int. J. Fatigue. **24**, 825–830 (2002)
36. DTU 10 MW Reference Wind Turbine Project Site: `http://dtu-10mw-rwt.vindenergi.dtu.dk`
37. Bak C., Zahle F., Bitsche R., Kim T., Yde A., Henriksen L.C., Andersen P.B., Natarajan A., Hansen M.H.: Design and performance of a 10 MW wind turbine. Wind Energy, to appear
38. Griffith D.T., Johanns W.: Large Blade Manufacturing Cost Studies Using the Sandia Blade Manufacturing Cost Tool and Sandia 100-meter Blades, Technical Report SAND2013-2734, (2013)